Estimating Rainfall Intensities from Weather Radar Data: The Scale-Dependency Problem

EFRAT MORIN

Department of Hydrology and Water Resources, The University of Arizona, Tucson, Arizona

WITOLD F. KRAJEWSKI

IIHR–Hydroscience and Engineering, University of Iowa, Iowa City, Iowa

DAVID C. GOODRICH

USDA–ARS, Southwest Watershed Research Center, Tucson, Arizona

XIAOGANG GAO AND SOROOSH SOROOSHIAN

Department of Hydrology and Water Resources, The University of Arizona, Tucson, Arizona

(Manuscript received 19 September 2002, in final form 31 January 2003)

ABSTRACT

Meteorological radar is a remote sensing system that provides rainfall estimations at high spatial and temporal resolutions. The radar-based rainfall intensities (R) are calculated from the observed radar reflectivities (Z). Often, rain gauge rainfall observations are used in combination with the radar data to find the optimal parameters in the Z–R transformation equation. The scale dependency of the power-law Z–R parameters when estimated from radar reflectivity and rain gauge intensity data is explored herein. The multiplicative (a) and exponent (b) parameters are said to be ''scale dependent'' if applying the observed and calculated rainfall intensities to objective function at different scale results in different ''optimal'' parameters. Radar and gauge data were analyzed from convective storms over a midsize, semiarid, and well-equipped watershed. Using the root-mean-square difference (rmsd) objective function, a significant scale dependency was observed. Increased time- and space scales resulted in a considerable increase of the a parameter and decrease of the b parameter. Two sources of uncertainties related to scale dependency were examined: 1) observational uncertainties, which were studied both experimentally and with simplified models that allow representation of observation errors; and 2) model uncertainties. It was found that observational errors are mainly (but not only) associated with positive bias of the b parameter that is reduced with integration, at least for small scales. Model errors also result in scale dependency, but the trend is less systematic, as in the case of observational errors. It is concluded that identification of optimal scale for Z–R relationship determination requires further knowledge of reflectivity and rain-intensity error structure.

1. Introduction

Rainfall estimation based on meteorological radar data is one of the most intensely studied topics by radar meteorologists and hydrologists (Atlas et al. 1997). The challenge is to produce accurate, high-resolution, large-extent rainfall-intensity and/or accumulation maps based on the radar data. These maps provide essential information for a variety of hydrologic applications, such as estimating and forecasting floods, streamflows, and water budgets.

Corresponding author address: Efrat Morin, Department of Hydrology and Water Resources, The University of Arizona, Tucson, AZ 85721.
E-mail: morine@hwr.arizona.edu

A key issue in radar-based rainfall estimation is to identify the relationships between reflectivity (Z) and rain intensity (R). In ideal conditions, reflectivity is closely related to backscattered radar energy from raindrops in the atmosphere. Both Z and R are defined as different moments of the drop size distribution (DSD) in a sampled volume (Sauvageot 1992). However, these definitions alone do not imply a straightforward functional relationship between the two variables. Studies in the past 60 yr indicate that on average Z and R can be related by a power law:

$$Z = aR^b, \tag{1}$$

where Z is reflectivity (mm^6 m^{-3}), R is rainfall intensity (mm h^{-1}), and a and b are empirical parameters. In an

© 2003 American Meteorological Society

Unauthenticated | Downloaded 04/15/21 10:46 AM UTC

early study, Marshall and Palmer (1948) found that the DSD is approximately exponential with a slope parameter that is a function of R, which leads to the power-law relation with the parameters $a = 200$ and $b = 1.6$. Many subsequent studies indicate a power-law Z–R relationship but suggest different values for the parameters (see, e.g., Battan 1973). Among those are $a = 300$, $b = 1.4$ [used in the United States in the Weather Surveillance Radar-1988 Doppler (WSR-88D) system for rainfall associated with deep convection], and $a = 250$, $b = 1.2$ (recommended for tropical rain events) (Rosenfeld et al. 1993). Typical values of the a parameter may range from a few tens to several hundreds, while b is usually limited to $1 \leq b \leq 3$ (Battan 1973; Smith and Krajewski 1993). The large variation in the parameters is attributed to different rain types associated with different DSDs, and to the statistical nature of the DSD, which varies widely between and within storms. Stable exponential DSDs, such as those found by Marshall and Palmer (1948) and others, are based on highly averaged data that hide some of the variability (Atlas et al. 1997). Therefore, while it is clear that physical processes related to the nature of precipitation affect the Z–R relationship, the statistical effects are no less important. Joss and Gori (1978) show that the shape of the DSD depends on sample size. Campos and Zawadzki (2000) found that the Z–R relation depends on instrument sensor and on the method for data analysis. Jameson and Kostinski (2001) claimed that Z–R relations are actually physically linear but are identified as power law because of statistical inhomogeneity. In spite of the above difficulties, and although in recent years other relations were suggested (e.g., Rosenfeld et al. 1994), the power-law Z–R still remains the most popular relationship used in research and in practice.

A major problem in estimating Z–R relations based on observations is that both variables are subjected to uncertainties. Steiner et al. (1999) show the effect of using erroneous rain gauge data on adjusted radar rain estimates, and Ciach and Krajewski (1999) examine the effect of observational radar–gauge errors on determined power-law parameters. Joss and Gori (1978) and Campos and Zawadzki (2000) examine uncertainties in distrometer data and their effect on the determined Z–R relation. A possible way to reduce some of the uncertainties is by space–time integration of rain intensities and/or reflectivities. As a result of the reduction in uncertainty, as well as for other reasons, the Z–R relation identified for the integrated data may be different from the one identified for the originally observed data. If so, we indicate that the Z–R relations are scale dependent. Although the effect of integration on observational errors was studied in the past (e.g., Zawadzki et al. 1986; Seed and Austin 1990; Ulbrich and Lee 1999; Jordan et al. 2000), its direct effect on the determined Z–R relation was not comprehensively examined.

The main purpose of our paper is to experimentally demonstrate the scale dependency of the power-law Z–R relation and to examine its causes for convective storms in the U.S. Department of Agriculture (USDA)-Agricultural Research Service (ARS) Walnut Gulch Experimental Watershed (WGEW), located in southeastern Arizona. The watershed is covered with a very dense network of rain gauges and has been the site of many previous hydrologic studies. The paper outline is as follows. In section 2 we describe the process of identifying power-law parameters based on observations and elucidate the meaning of scale dependency in this context. In section 3 we give details about the study area, the data, selected storms, and the analysis methods. In section 4 we present and discuss the analysis results. We examine the causes of the scale dependency found using both observations and rainfall models, which allow representation of observational errors. We close with concluding remarks in section 5.

2. Identification of Z–R power-law relations at different scales

The analysis of observations is an integral part of identifying Z–R relations. Often, rain gauge rainfall observations are used in combination with the radar data to find the most appropriate a and b parameters to be used in a power-law function [Eq. (1)]. The form of the Z–R power law in Eq. (1) is the conventional way of representing this relationship; however, since it is used for estimating rainfall intensities (R) from the *observed* reflectivities (Z), the more appropriate form is

$$R = \left(\frac{1}{a}\right)^{1/b} Z^{1/b}. \tag{2}$$

[See Ciach and Krajewski (1999) and Campos and Zawadzki (2000) for illustrations of the implication of expressing the relationship in this form.] The optimal a and b parameters are then estimated from measurements of radar reflectivity and gauge rainfall intensity. The fit between the observed gauge and estimated radar rainfall intensities is evaluated using some objective function. The parameters that optimize this function are selected. For example, the root-mean-square difference (rmsd) is a commonly used objective function, defined by

$$\text{rmsd} = \sqrt{\frac{1}{n}\sum_{i=1}^{n}(G_i - R_i)^2}, \tag{3}$$

where G_i is the observed gauge rainfall intensity, R_i is the estimated radar rainfall intensity with given values of a and b, and n is the number of data pairs compared. The optimal a and b parameters are those that minimize the rmsd function. In addition to the rmsd, other possible objective functions are the mean absolute difference, the conditional bias (Ciach et al. 2000), and others. Also, in many studies rmsd is used with log transformation of Eq. (1), which makes it linear, but introduces other difficulties (see section 4c, e.g.).

Unauthenticated | Downloaded 04/15/21 10:46 AM UTC

We focus on scale dependency of the power-law function parameters using the rmsd objective function. For example, the rmsd can be calculated between hourly integrated gauge rainfall and hourly integrated radar rainfall. The a and b parameters that minimize the rmsd with the hourly integration are those that generate the best (in terms of the rmsd) estimates of radar-derived hourly rainfall. In general, for a given timescale T and a space scale S,

$$\text{rmsd}_{\text{TS}} = \sqrt{\frac{1}{n_{\text{TS}}} \sum_{i=1}^{n_{\text{TS}}} (G_{\text{TS}_i} - R_{\text{TS}_i})^2}, \qquad (4)$$

where G_{TS_i} is the observed gauge rainfall intensity integrated to timescale T and space scale S, R_{TS_i} is the calculated rainfall intensity integrated to timescale T and space scale S for given a and b parameters, and n_{TS} is the number of compared values in these specific time- and space scales. As before, the optimal a and b parameters for timescale T and space scale S are those that minimize the rmsd_{TS} function. The parameters are said to be scale dependent if their optimal values change with scale, which means that there are different optimal parameters for different scales.

The space–time integration of the radar data can be performed for the rainfall intensities, as we presented above, or for the reflectivity data. In the first case, which we term $R(Z)$ averaging, the Z–R transformation is applied to the highest-resolution reflectivity data (the measurement scale), and then the calculated rainfall intensities are integrated to the specific time- and space scales. In the second case, which we term Z averaging, the radar reflectivity (in terms of Z) is integrated and the Z–R transformation is applied to the integrated reflectivities. The two cases result in different optimal solutions due to the nonlinear nature of the Z–R transformation and represent two different goals of optimization. In $R(Z)$ averaging, the observations are collected at the same scale, but we wish to optimize the rain-intensity estimations for different scales for different applications. On the other hand, Z averaging represents the comparison of Z–R based on different measuring devices with different domain size and interval.

We also emphasize that the two parameters in the power-law relations are not independent of each other. In fact, by deriving (4) with respect to a it can be shown that for any given $b = b_0$, (4) is minimized with $a = a_0$:

$$a_0 = \left[\frac{\sum_{i=1}^{n_{\text{TS}}} G_{\text{TS}_i} R(1, b_0)_{\text{TS}_i}}{\sum_{i=1}^{n_{\text{TS}}} R(1, b_0)^2_{\text{TS}_i}} \right]^{-b_0}, \qquad (5)$$

where $R(1, b_0)_{\text{TS}}$ is the calculated rainfall intensity integrated to timescale T and space scale S with parameters $a = 1$ and $b = b_0$. Equation (5) implies that a is a function of the dataset, the desired scale, and b. For that reason, in some of the analysis we show the effect on b only. Note that Eq. (5) does not guarantee removal of bias between radar- and gauge-derived rainfall.

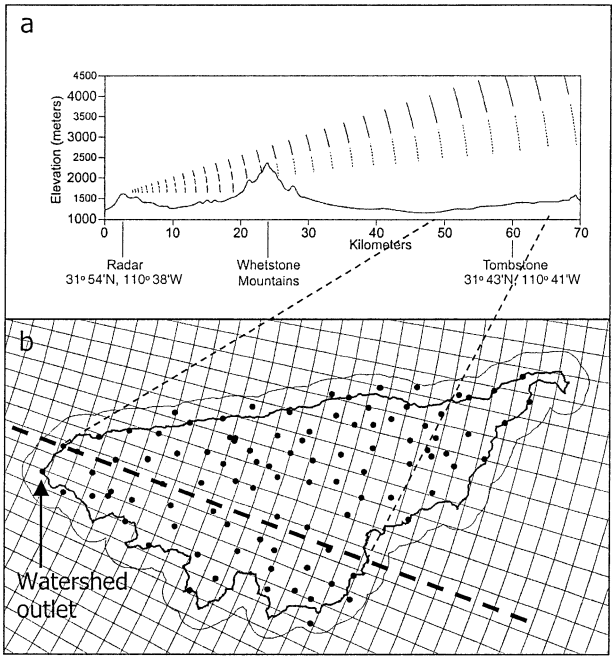

FIG. 1. (a) Vertical profile view of the axis between the Tucson, AZ radar system and the Walnut Gulch Watershed (Tombstone, AZ) and the blockage in the two lowest radar elevation angles. (b) Rain gauge network (74 gauges passed the quality control), radar cells (1°, 1-km resolution), and 1-km buffer around the watershed boundary. Thick dashed line shows the axis line at which the vertical profile was generated, which extends 110° clockwise from radar north.

3. Data and methodology

a. Study area

Ground rainfall observations were obtained from a dense network of rain gauges located in and near the 149 km^2 USDA-ARS WGEW (31°43′N, 110°41′W) (Fig. 1). Elevation of the watershed ranges from 1250 to 1585 m MSL. Mean annual temperature at Tombstone, Arizona, located within the watershed, is 17.6°C, and mean annual precipitation is 324 mm, with considerable seasonal and annual variation in precipitation. Osborn (1983) reported, based on records from 1956–80, that annual precipitation varied from 170 mm in 1956 to 378 mm in 1977; summer rainfall varied from 104 mm in 1960 to 290 mm in 1966; and winter precipitation varied from 25 mm in 1966/67 to 233 mm in 1978/79. Approximately two-thirds of the annual precipitation occurs as high-intensity, convective thunderstorms of limited areal extent. Winter rains (and occasional snow) are generally low-intensity events associated with large-scale cyclonic storms embedded in the prevailing westerlies (Sellers and Hill 1974) and are typically of greater areal extent than summer rains. Run-

Unauthenticated | Downloaded 04/15/21 10:46 AM UTC

TABLE 1. Selected storms' characteristics (based on gauge data).

Storm	Local start time	Duration (h)	Areal storm depth[a] (mm)	Max 1 min[b] (mm h^{-1})	Max depth[c] (mm)
1	17 Jun 1999 1400	2	2.4	150	27.9
2	25 Jun 1999 1400	4	0.9	47	5.6
3	6 Jul 1999 1100	12	11.3	148	29.1
4	14 Jul 1999 1100	28	48.9	260	93.3
5	25 Jul 1999 1700	3	1.6	232	25.6
6	2 Aug 1999 1600	6	10.7	152	29.8
7	18 Aug 1999 1400	2	2.4	166	16.2
8	28 Aug 1999 1700	5	20.4	230	38.3
9	31 Aug 1999 1500	5	17.1	219	49.1
10	16 Sep 1999 1700	7	6.0	136	25.9
11	18 Jun 2000 1600	3	3.3	129	24.3
12	29 Jun 2000 1100	4	15.5	182	58.3
13	16 Jul 2000 1700	6	7.6	113	30.7
14	6 Aug 2000 1900	6	25.6	326	56.7
15	11 Aug 2000 1200	4	24.9	391	91.2

[a] All-gauges average.
[b] Maximum 1-min rainfall intensity recorded at a gauge.
[c] Maximum storm depth recorded at a gauge.

off is generated almost exclusively from convective storms during the summer monsoon season via infiltration excess. Using the modified Koppen method (Trewartha 1954), the climate at Tombstone is classified as semiarid or steppe with a dry winter but is quite close to being an arid or desert climate. For a more detailed description of the WGEW see Renard et al. (1993), Kustas and Goodrich (1994), or Goodrich et al. (1997).

The initial rainfall and runoff instrumentation on Walnut Gulch was installed in 1954–55 and was expanded in the early 1960s to the 85-gauge network currently in place on the watershed (Osborn and Reynolds 1963). This network enabled the first detailed characterization of airmass thunderstorms in the Southwest and has resulted in a significant body of research on this type of storm phenomena (Osborn and Reynolds 1963; Osborn and Hickok 1968; Osborn et al. 1972; Osborn and Lane 1972; Osborn and Laursen 1973; Smith 1974; Osborn et al. 1979; Eagleson et al. 1987; Osborn and Renard 1988). Even though the rain gauge mechanical clocks were calibrated on a yearly basis, time synchronization across the network was not better than roughly a 5–10-min interval. To overcome these limitations and others the USDA-ARS Southwest Watershed Research Center (SWRC) began a watershed instrumentation modernization effort in the mid-1990s. The staff of the SWRC developed a new load-cell-weighing rain gauge designed to record at 1-min time intervals on modern dataloggers with significantly smaller timing errors. This was accomplished using telemetry commands in which all the datalogger times are set to coordinated universal time (UTC) every 24 h. With this approach, synchronization errors between functioning rain gauges are typically several seconds or less and absolute time errors may be on the order of 5–10 s. The new digital rain gauge network became fully operational in 1999, 3 yr after the Tucson Doppler radar became operational.

b. Rain gauge data processing and storm selection

Detailed examination of the rain gauge data resulted in elimination of 11 rain gauges for quality control purposes. Observations from 74 rain gauges were compared to radar-derived rainfall observations. Since some of the WGEW rain gauges are located on the watershed boundary or just outside of it, we added a buffer of 1 km to the watershed boundary (Fig. 1b). The studied area was therefore increased to 220 km^2.

The digital rain gauges have a threshold sensitivity requiring 0.254 mm (0.01 in.) of rainfall depth to be exceeded before the gauge starts to record data. This threshold implies that 1-min rainfall intensities lower than 15.2 mm h^{-1} (0.254 mm min^{-1}) are not accurate, because the exact duration of the rain depth that is lower than the threshold is not known. We assumed the first 0.254 mm appearing after a period of no data to be equally spread over the duration of time since the preceding record, but no longer than 15 min. Similar to tipping-bucket gauges (Habib et al. 2001), there is significant uncertainty associated with low rainfall intensities due to limited sensitivity of the instrument.

Fifteen convective storms from the 1999 and 2000 summer monsoon seasons were selected for in-depth analysis. The selected group of storms represents the airmass thunderstorms typical of the U.S. Southwest. Selected characteristics of these storms are contained in Table 1. All 15 storms contain high rainfall intensities and are characterized by high spatial variability. The 15 storms have a total of 199 mm of rainfall. The maximum 1-min intensity and maximum storm depth recorded by any single gauge range from 47 to 391 mm h^{-1} and from 6 to 93 mm, respectively. Correlation coefficients of rain intensities for 5, 15, 30, and 60 min based on data from all 15 storms are presented in Fig. 2. At 1-km gauge separation distance the average correlation

Unauthenticated | Downloaded 04/15/21 10:46 AM UTC

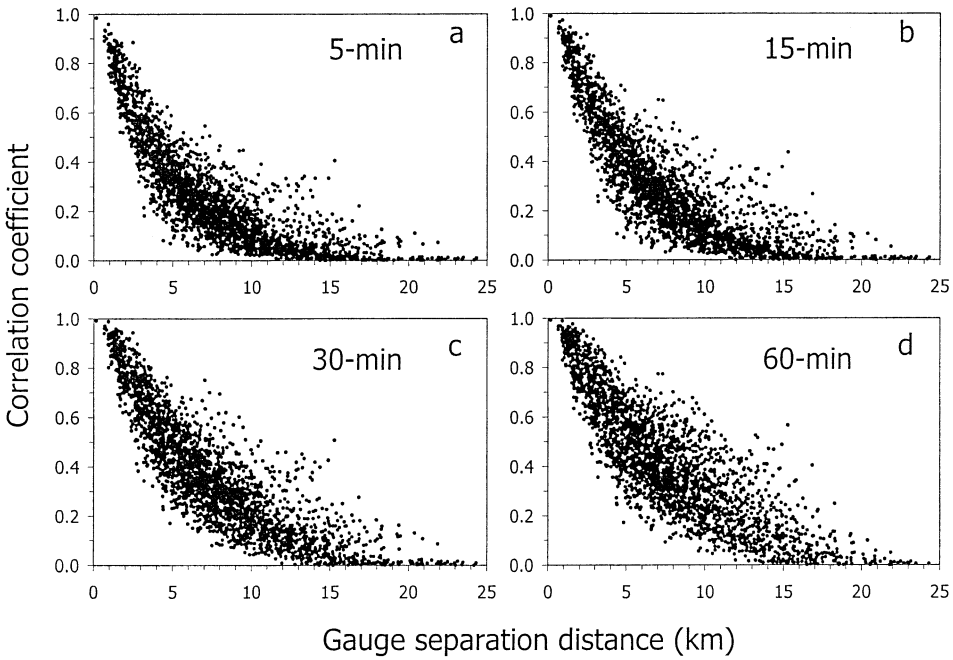

FIG. 2. Correlation of gauge rain intensities as a function of gauge-separation distance. The analysis is based on the 15 storms used in this study for durations of (a) 5, (b) 15, (c) 30, and (d) 60 min.

coefficients are 0.84, 0.87, 0.90, and 0.91 for 5-, 15-, 30-, and 60-min rain intensities, respectively. At 3-km gauge separation distance the correlations are reduced to 0.53, 0.59, 0.68, and 0.71, respectively, for the same durations.

c. Radar data processing

The radar data used in the analysis are the Level II reflectivity data from the Tucson WSR-88D radar (31°54′N, 110°38′W; 1616 m MSL). The watershed is located 50–70 km east-southeast of the radar (see Fig. 1a). At this distance, the area of the basic radar cells over the watershed is in the range of 0.88 to 1.23 km^2 (1° in azimuth and 1-km radial length). The radar completes a volume scan in about 5 min. The lowest scan elevation angle (0.5°), as well as a large part of the second tilt (1.5°) is blocked by terrain over the entire WGEW (see Fig. 3). Therefore, data from the third scan angle (2.4°) were used for the analysis. The elevation of these radar data above the WGEW is approximately 3000 m on average.

The relatively high altitude of the radar data above the surface is known to impose some difficulties that need to be addressed. The first difficulty is the possible presence of hail particles aloft, which results in high radar reflectivity returns. We dealt with this problem by using the operational approach, which applies an upper threshold to the reflectivity data, with the common value of 53 dB*Z*. Comparison of occurrences of high reflectivities with occurrences of high observed gauge intensities in a reasonable distance and time delay is presented in Fig. 4. For each radar pixel, the conditional probability (over all 15 storms) of rain intensity is shown to be equal to or larger than 104 mm h^{-1} at a gauge located at a distance of no more than three pixels and within the 10 min following the radar recording time, given that the reflectivity equal to or larger than 53 dB*Z* is observed at the pixel. The threshold rain-intensity value of 104 mm h^{-1} was selected according to Eq. (2) with $Z = 53$ dB*Z*, $a = 300$, and $b = 1.4$. Only radar pixels that have at least one gauge in each quadrant are included in the analysis. Out of the 1115 occurrences of high reflectivity, 986 were associated with high ground rain intensity (88%). Based on this result, we suggest that, after applying the upper threshold to the reflectivity data, hail contamination has no significant effect on the analysis presented in the paper.

Another problem caused by the high altitude of the radar observations is the difference between reflectivities aloft and at the surface, both in value and in location and timing. The first is a result of vertical gradients, which can be caused by evaporation (typically high in the region) among other reasons. The second results from horizontal advection and can cause synchronization errors of 5–15 min in time and a few kilometers in space that may vary between storms. The effect of synchronization errors on scale dependency is examined in the analysis presented in section 4b.

We would like to emphasize that, although the use of the third tilt radar data may result in the above sources of uncertainties (caused by advection, vertical profile changes, evaporation, and hail contamination), these uncertainties exist in any operational or research radar–

Unauthenticated | Downloaded 04/15/21 10:46 AM UTC

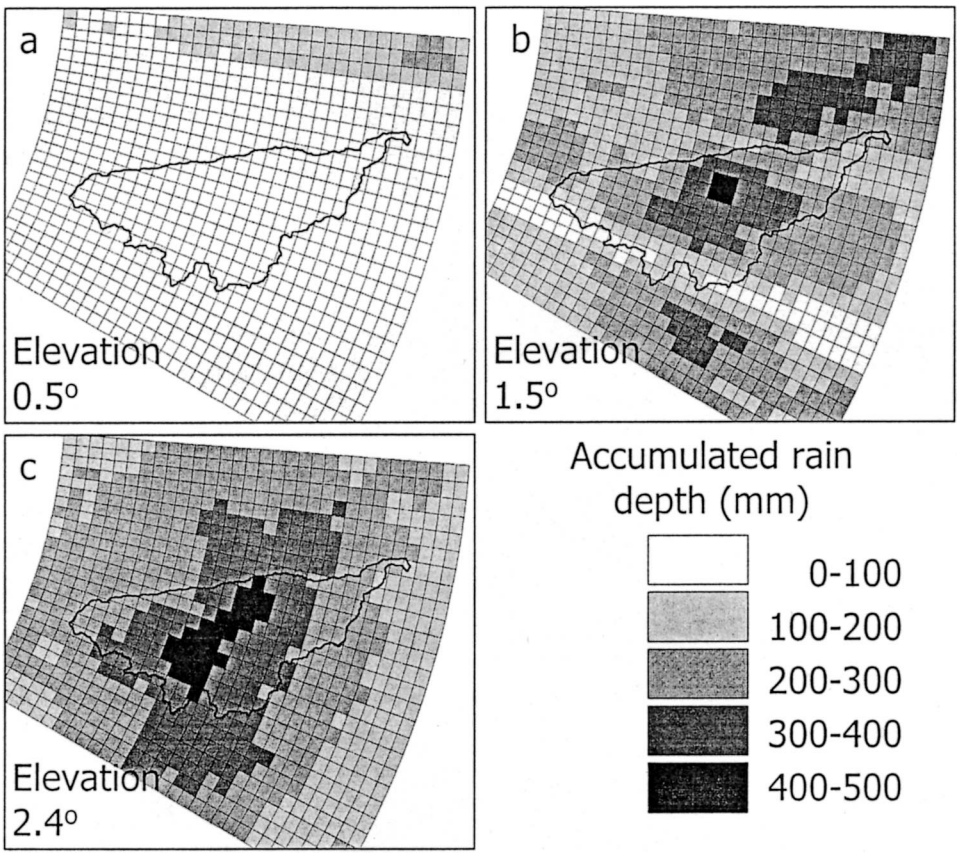

FIG. 3. Accumulated rain depth for 15 storms calculated from radar data using the $Z = 300R^{1.4}$ relationship for the first three radar tilts: (a) 0.5°, (b) 1.5°, and (c) 2.4°. The blockages of the first and the second (partially) tilts are evident.

gauge dataset. For example, in the precipitation product of the National Weather Service, data from the best out of the lowest four radar tilts are used (in terms of blockage and ground clutter). The complex terrain in the western United States implies that a large part of the precipitation product is based on data from 3 km or more above ground level (see Maddox et al. 2002).

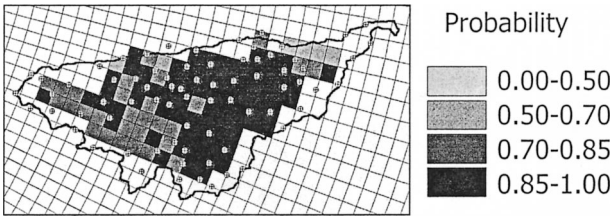

FIG. 4. For each radar pixel, the conditional probability (over all 15 storms) of rain intensity to be equal to or larger than 104 mm h^{-1} at a gauge located no farther than three pixels distance and within the 10 min following the radar recording time, given that reflectivity equal to or larger than 53 dBZ is observed at the pixel. Only radar pixels that have at least one gauge in each quadrant are included in the analysis. The value of $R = 104$ mm h^{-1} corresponds to $Z = 53$ dBZ assuming a power-law relationship with parameters $a = 300$ and $b = 1.4$. Gauge location is marked by plus sign.

d. Time and space integration

In the analysis, we integrated radar and gauge data at different time- and space scales. We describe the integration method used for each data type below. However, it should be noted that, because of the high variability of rainfall in space and time (especially in semiarid environments; see Fig. 2, e.g.), there are significant uncertainties in the value of the integrated rainfall.

For spatial integration we utilized Cartesian grids ranging from 1×1 km^2 to 5×5 km^2. To map the radar rainfall data from the polar to the Cartesian grid we calculated the area-weighted sum of the radar data in each grid cell. For spatial integration of gauge data, we first generated a high-resolution grid (100×100 m^2 cell size), calculating the cell values using the gauge point data. For each 100×100 m^2 grid cell, we interpolated the data of the four closest gauges, one in each quadrant, using the inverse distance weighing (IDW) method (e.g., Creutin and Obled 1982). We then integrated the 100×100 m^2 grid to the desired spatial scale. The interpolation was conducted only within the extended catchment (Fig. 1b), weighting the contributions from the grids according to their area.

Unauthenticated | Downloaded 04/15/21 10:46 AM UTC

For temporal integration, we calculated equal time-interval data (for each grid cell), for timescales of 5, 10, 15, 20, 30, 60, and 120 min. We generated these data by averaging the 5-min intervals for the WSR-88D radar data and the 1-min intervals for the gauge data. For each storm the data include the duration of observed rain within the catchment (by gauge or radar), extended (with zeros) to include an even number of hours. As a result, each storm contains a whole number of time intervals for all the examined timescales.

4. Study results and discussion

a. Scale dependency of the power-law parameters

Using all the radar–rain gauge observation pairs from the 15 storms selected (see Table 1) we estimated the optimal parameters a and b for space scales of 1, 2, 3, 4, and 5 km and timescales of 5, 10, 15, 20, 30, 60, and 120 min. Figure 5 shows the optimal parameters for the examined time- and space scales for the two types of averaging (see section 2). It is clearly shown that the a and b parameters are scale dependent, because they are shifted in parameter space systematically as the time- and space scales change (Fig. 5a). For $R(Z)$ averaging (Fig. 5b), parameter b decreases as scale increases from 5 to 120 min and from 1 to 5 km. In the case of Z averaging (Fig. 5c), b generally decreases by up to 30 min and then starts to increase. Figure 5a also demonstrates dependency between the a and b parameters. In general we see that as b decreases a increases. This type of dependency is known and has been reported previously (Ciach et al. 1997). The optimal parameters for the two types of averaging are different. For Z averaging the optimal b parameter tends to be smaller. This is not surprising since the power-law relation is not linear.

Figures 6 and 7 present comparison of gauge rain intensities with radar rain intensities [$R(Z)$ averaged] obtained with the determined optimal parameters for four selected time- and space scales. Figure 6 shows a scatterplot of the gauge and radar rain intensities, and Fig. 7 shows distribution of the residuals. At very small scales (1 km, 5 min; Fig. 6a) the scatter is large and the relationships between the gauge and radar data are very weak, especially for gauge rain intensities lower than 50 mm h^{-1}. In addition, for gauge intensities higher than 50 mm h^{-1} there is an underestimation by the radar. As scale increases, the scatter is reduced and a better fit between the gauge and radar rain intensities is observed (Figs. 6b–d). Figure 6 also demonstrates why higher values of b are better fitted to data with large scatter. Consider a situation where the radar reflectivity and gauge intensity are totally uncorrelated. In that case, the best-fit curve is a constant radar rain intensity equal to the average gauge rain intensity. For radar intensity to be as close as possible to constant, b must be as large as possible [Eqs. (1) and (2)] We examine in detail the effect of data errors on the optimal parameters in the next section.

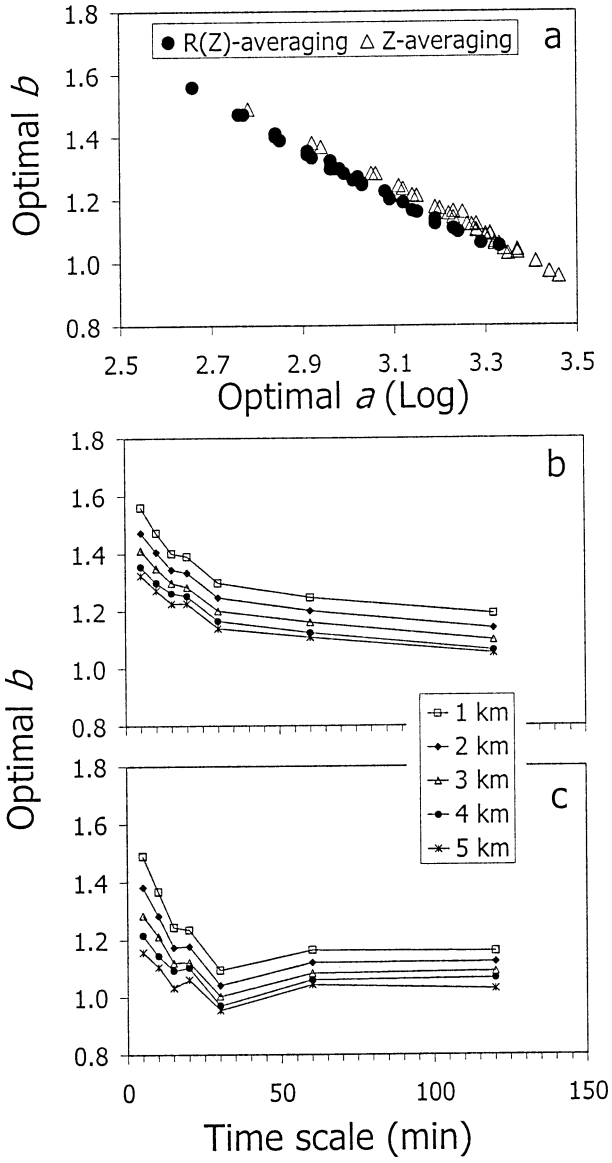

FIG. 5. (a) The a–b parameters space (a represented in log scale) with points indicating the optimal power-law parameters for the examined time- and space scales for the two types of averaging: $R(Z)$ averaging (filled circles) and Z averaging (open triangles). (b) Change of the optimal b parameter with timescale using $R(Z)$ averaging. Each line represents a specific space scale. (c) Same as (b) but for Z averaging.

In the above analysis the scale dependency of the a and b parameters is examined for the 15 storms as one group. In a second step, the same analysis is conducted for individual storms and for groups of three and five storms. Figure 8 presents the change in the optimal parameter b with timescale (for space scale 1 km), for separate storms and groups of storms. When single storms are analyzed (Fig. 8a) we see a large diversity of the parameter value. Although part of this diversity

Unauthenticated | Downloaded 04/15/21 10:46 AM UTC

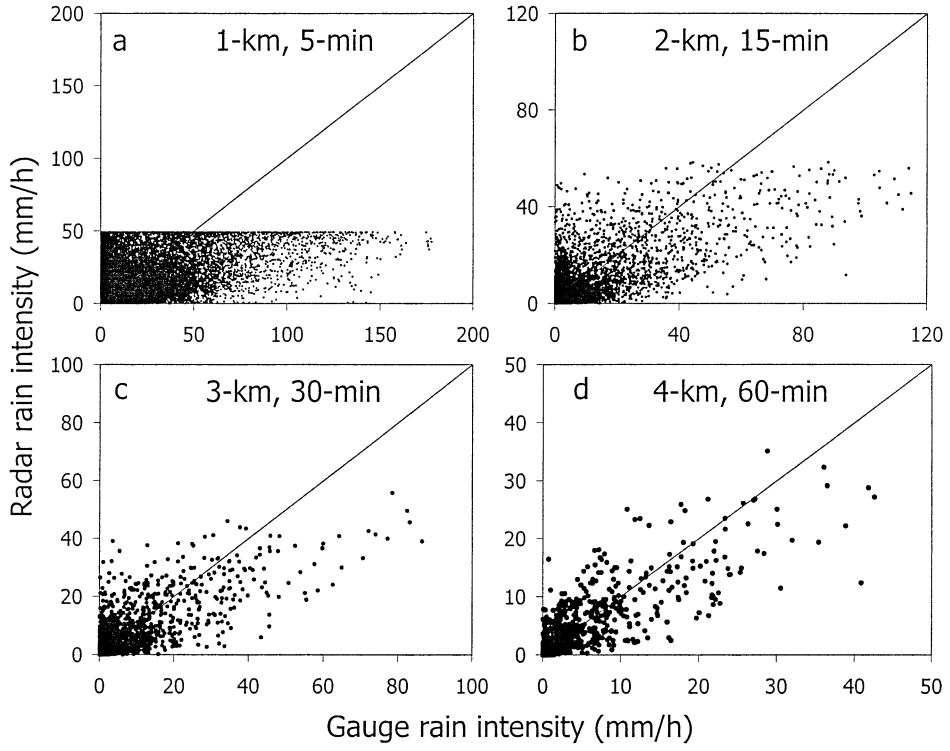

FIG. 6. Gauge rain intensities compared with radar-based rain intensities using optimal parameters for four space–time scales: (a) 1 km, 5 min, $a = 458$, $b = 1.56$; (b) 2 km, 15 min, $a = 821$, $b = 1.34$; (c) 3 km, 30 min, $a = 1239$, $b = 1.20$; and (d) 4 km, 60 min, $a = 1563$, $b = 1.12$.

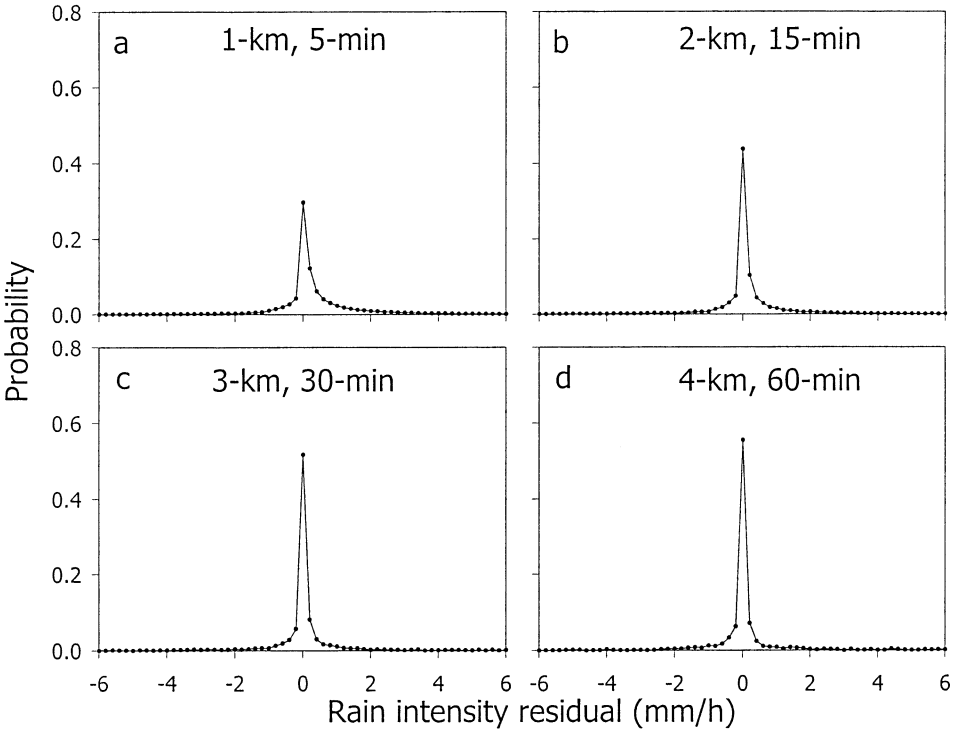

FIG. 7. Histogram of residuals for the same four space–time scales as in Fig. 6.

Unauthenticated | Downloaded 04/15/21 10:46 AM UTC

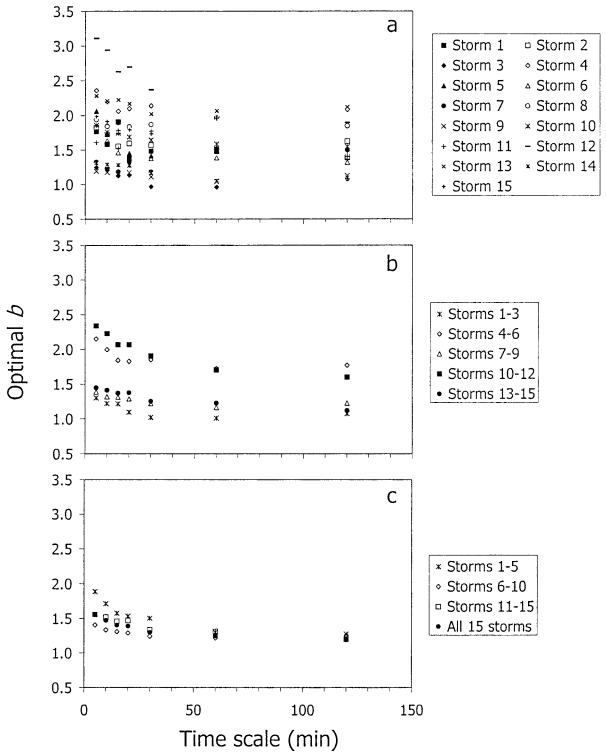

FIG. 8. Analysis of scale dependency of parameter *b* for (a) each storm separately, (b) groups of three storms, and (c) groups of five storms.

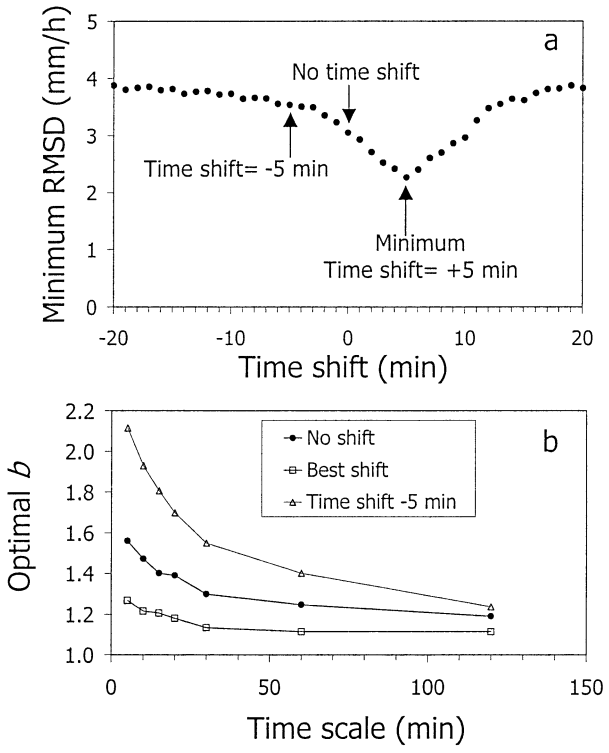

FIG. 9. (a) The effect of time shifting of the radar data on the minimum value of the rmsd objective function for the 17 Jun 1999 storm. (b) Change of the optimal *b* parameter with timescale for different time shifts of the radar data. Open squares represent the best space–time shift for each storm. Filled circles and open triangular symbols represent no time shift and a −5 min time shift, respectively.

could be attributed to differences in the storm's nature, it is more likely that the sample size of one-storm data is not large enough for identifying stable parameters. As sample size increases (by grouping the storms) the diversity is reduced. The integration also reduces the span of the parameters.

b. Observational errors effect

Observational errors include errors in radar measurement of reflectivity (resulting from blockage, attenuation, partial beam filling, hardware problems, and others), errors in gauge measurement of rain intensity, errors in interpolation to the desired time- and space scales, synchronization errors, errors between reflectivity aloft to near-surface reflectivity, etc. Some of the errors are reduced with scale. Here we consider synchronization errors as an example. Synchronization errors evolve from the different altitudes at which radar and gauge data are measured. The data observed by the radar aloft is associated with rain intensity at the ground with some time delay and shift in space. The magnitude of these time–space shifts depends on the vertical velocity of the raindrops and the horizontal advection. In the current case study, with a 3-km vertical difference between radar and gauge data, we can expect a time lag on the order of 5–15 min (radar data precede gauge data) and horizontal displacement of 3–9 km. Synchronization errors in the data were identified by examining how the minimum of the rmsd function varied for different shifts of the radar data in time and space. Comparison was done between 3-min gauge rain intensity and radar data at the pixel above the gauge (after applying a space shift). For example, in the 17 June 1999 storm (Fig. 9a), the time shift that minimizes the rsmd is +5 min. Using radar data that are 5 min later than the recorded time provides, therefore, the best match between the radar and gauge rain intensities. In the same way, the best time and space shifts for each of the studied storms were found. For all but two storms we found clearly determined best shifts in the range of 0–4 km in space and 3–9 min in time [these results agree qualitatively with those obtained by Habib and Krajewski (2002)]. For two storms (storms 2 and 5 in Table 1) a clear best shift could not be identified. Although including these storms in the analysis did not change the results, they were excluded from the following analysis for consistency.

We investigated the change in *b* with scale for three levels of synchronization error: 1) no shift, 2) the best shift for each storm, and 3) a −5 min shift for all storms. The negative time shift in the third level increases the synchronization error because we use the radar data ear-

Unauthenticated | Downloaded 04/15/21 10:46 AM UTC

lier than their recorded times, which already precede the gauge times by several minutes (see Fig. 9a). Figure 9b illustrates that as radar–gauge synchronization errors are minimized the change in b with timescale is minimal. On the other hand, when error is enhanced (a negative time shift is applied) the change in b is larger. In summary, these results demonstrate a close relation between scale dependency and observational errors. Moreover, they suggest that the estimated exponent parameter b is positively biased by the errors, and this bias is reduced with scale as the level of error decreases.

Using two simplified rainfall models, we examine next the effect of observational error and changes of scale on the b-parameter bias. In the first model, we use the log transformation for Z and R with linear regression theory to estimate the parameters in Eq. (1). Although used quite often, regression of the log function for estimating the power-law parameters should be done with caution. This is because the optimal parameters might be different from those identified by nonlinear regression, and zeros cannot be handled by the log transformation.

The model assumes that the ''true'' Z and R are related to each other through a power law [Eq. (1)], but each one of the variables is independently corrupted by a multiplicative observational error. Using the log transformation for Z and R we get

$$\log(R_{\text{tr}}) = \left[-\frac{\log(a)}{b}\right] + \frac{1}{b}\log(Z_{\text{tr}}),$$

$$\log(R_{\text{ob}}) = \log(R_{\text{tr}}) + \varepsilon, \qquad \log(Z_{\text{ob}}) = \log(Z_{\text{tr}}) + \delta, \tag{6}$$

where the abbreviations tr and ob stand for the true and observed variables, respectively. The error variables ε (of rain intensity) and δ (of reflectivity) are assumed to be independent of each other and for the different observations and to be normally distributed with zero mean and constant variance:

$$\varepsilon \sim N(0, \sigma^2),\ \delta \sim N(0, \sigma_\delta^2). \tag{7}$$

Following linear regression theory with errors in the predictor (Draper and Smith 1981), the b parameter is estimated with a bias with respect to the true parameter b_0:

$$E(\hat{b}) = b_0\left[1 + \frac{\sigma_\delta^2 + \sigma_{\log(Z_{\text{tr}})\delta}}{\sigma^2_{\log(Z_{\text{tr}})} + \sigma_{\log(Z_{\text{tr}})\delta}}\right], \tag{8}$$

where $\sigma^2_{\log(Z_{\text{tr}})}$ is the variance of $\log(Z_{\text{tr}})$ and $\sigma_{\log(Z_{\text{tr}})\delta}$ is the covariance of $\log(Z_{\text{tr}})$ and δ. Due to the assumption of independence of errors in reflectivity and in rain intensity, the latter do not affect the bias. Each of the three terms in the bias factor in Eq. (8) changes with scale. We use reflectivity time series data from one radar pixel (at the watershed's center) as the true reflectivity, and we contaminant the data with three types of observational errors: 1) random error (3 dBZ), 2) synchronization error (5-min time shift), and 3) hail contamination. The hail contamination error is generated by keeping the reflectivities above the 53-dBZ hail threshold (see section 3c) with their original observed value and assuming that 53 dBZ is the true reflectivity. Rainfall intensities are simulated (with no error) as a power law of the true reflectivity with $a = 300$ and $b = 1.4$. For each timescale, the reflectivity and the rain intensity data are averaged (Z averaging for the radar data) and the linear regression is applied to the averaged time series. Table 2 contains the parameters found by regression of rain intensity with the true reflectivity (indicated by a_{tr} and b_{tr}) and the parameters found by regression with the erroneous reflectivity time series (indicated by a_{ob} and b_{ob}). The variances and covariance terms in Eq. (8) and the bias factor are also contained in the table. The bias factor is calculated from Eq. (8) and also is derived by the ratio $b_{\text{ob}}/b_{\text{tr}}$. As can be seen in the table, there are no differences between the two. The slight change in b_{tr} with scale is due to nonlinearity. Among the three types of error examined, the synchronization error has the largest effect on the estimated exponent. There is an overestimation of b (bias larger than 1) at the small scale and it is reduced with scale by up to 30 min and then increases. This is a result of reduction in the variance of the error, σ_δ^2, and the increase in variance of log reflectivities, $\sigma^2_{\log(Z_{\text{tr}})}$, as scale increases from 5 to 30 min. The resulting effect of fast reduction in the estimated b parameter at scales smaller than 30 min fits the trend found based on analysis of observed radar reflectivity and gauge intensity (see Fig. 5c).

The second rainfall model we use to examine the effect of error and scale on bias of the b parameter is previously described by Ciach and Krajewski (1999). It assumes multiplicative errors in rain intensity and reflectivity and uses nonlinear regression to estimate Z–R power-law parameters. The intensity and reflectivity variables and their associated errors are postulated to have lognormal distributions with mean 1 and constant variability as well as to be independent of each other. The resulting bias of b is

$$E(\hat{b}) = b_0\left[1 + \frac{\log(\sigma_\tau^2 + 1)}{\log(\sigma^2_{Z_{\text{tr}}} + 1)}\right], \tag{9}$$

where $\sigma^2_{Z_{\text{tr}}}$ is the variance of reflectivities and σ_τ^2 is the variance of the errors of reflectivity (in the multiplicative form). The independence assumed implies zero covariance of the reflectivities and their errors, $\sigma_{Z_{\text{tr}}}$.

We used the same dataset as for the first model to estimate the a and b parameters for the same three types of error. Table 3 contains the analysis for a nonlinear regression model. As in the linear model, the positive bias at the small scale is reduced with integration, at least initially. In the nonlinear model, however, the actual bias (the ratio $b_{\text{ob}}/b_{\text{tr}}$) is different from the bias according to Eq. (9). For the random and hail contam-

Unauthenticated | Downloaded 04/15/21 10:46 AM UTC

TABLE 2. Estimated parameters and statistics using a linear regression model.

Timescale (min)	N	a_{tr}^{*}	b_{tr}^{*}	a_{ob}^{**}	b_{ob}^{**}	$\sigma^{**}_{\log(Z_{tr})}$	σ^{**}_{δ}	$\sigma_{\log(Z_{tr})\delta}$	Bias [Eq. (8)]	b_{ob}/b_{tr}
Random error 3 dBZ										
5	2064	300	1.40	320	1.41	7.376	0.030	0.020	1.007	1.007
10	1032	326	1.41	348	1.41	7.707	0.018	0.012	1.004	1.004
15	688	348	1.41	367	1.42	7.986	0.014	0.005	1.002	1.002
20	516	364	1.42	382	1.42	8.121	0.012	−0.003	1.001	1.001
30	344	396	1.43	420	1.43	8.515	0.010	0.006	1.002	1.002
60	172	464	1.44	502	1.44	9.115	0.008	0.015	1.003	1.002
120	86	568	1.45	620	1.46	9.081	0.008	0.021	1.003	1.003
240	43	668	1.45	716	1.45	6.893	0.008	0.001	1.001	1.001
Synchronization error 5 min										
5	2064	300	1.40	805	1.54	7.376	1.378	−0.689	1.103	1.103
10	1032	326	1.41	561	1.49	7.707	0.804	−0.387	1.057	1.056
15	688	348	1.41	551	1.48	7.986	0.841	−0.463	1.050	1.049
20	516	364	1.42	610	1.49	8.121	0.678	−0.287	1.050	1.049
30	344	396	1.43	562	1.47	8.515	0.501	−0.263	1.029	1.029
60	172	464	1.44	751	1.48	9.115	0.615	−0.337	1.032	1.032
120	86	568	1.45	1020	1.51	9.081	0.922	−0.576	1.041	1.040
240	43	668	1.45	956	1.43	6.893	0.788	−0.877	0.985	0.984
Hail contamination										
5	2064	300	1.40	307	1.40	7.376	0.001	0.013	1.002	1.002
10	1032	326	1.41	335	1.41	7.707	0.001	0.017	1.002	1.002
15	688	348	1.41	357	1.42	7.986	0.001	0.018	1.002	1.002
20	516	364	1.42	379	1.42	8.121	0.002	0.027	1.004	1.003
30	344	396	1.43	412	1.43	8.515	0.002	0.028	1.004	1.004
60	172	464	1.44	495	1.45	9.115	0.004	0.049	1.006	1.006
120	86	568	1.45	621	1.46	9.081	0.006	0.071	1.008	1.008
240	43	668	1.45	750	1.47	6.893	0.010	0.086	1.014	1.013

* Parameters found by regression of the true time series.
** Parameters found by regression of the erroneous time series.

Unauthenticated | Downloaded 04/15/21 10:46 AM UTC

TABLE 3. Estimated parameters and statistics using a nonlinear regression model.

Timescale (min)	N	a_{tr}^{*}	b_{tr}^{*}	a_{ob}^{**}	b_{ob}^{**}	$\sigma_{Z_{tr}}^{**}$	σ_{τ}^{**}	$\sigma_{Z_{tr}\tau}$	Bias [Eq. (9)]	b_{ob}/b_{tr}
Random error 3 dBZ										
5	2064	300	1.40	135	1.65	3.450E + 08	0.179	3.282E + 02	1.008	1.179
10	1032	372	1.36	227	1.54	2.866E + 08	0.106	3.164E + 02	1.005	1.132
15	688	430	1.33	285	1.49	2.655E + 08	0.078	3.350E + 02	1.004	1.120
20	516	444	1.33	311	1.48	2.223E + 08	0.070	3.031E + 02	1.004	1.113
30	344	597	1.26	678	1.28	1.941E + 08	0.055	2.942E + 02	1.003	1.016
60	172	533	1.33	493	1.42	1.039E + 08	0.049	2.508E + 02	1.003	1.068
120	86	764	1.23	703	1.33	7.407E + 07	0.052	1.897E + 02	1.003	1.081
240	43	775	1.27	769	1.36	3.843E + 07	0.061	1.168E + 02	1.003	1.071
Synchronization error 5 min										
5	2064	300	1.40	74	1.85	3.450E + 08	9.275E + 12	−2.986E + 08	2.519	1.321
10	1032	372	1.36	123	1.70	2.866E + 08	7.656E + 11	−8.323E + 07	2.405	1.250
15	688	430	1.33	353	1.41	2.655E + 08	5.100E + 11	−8.239E + 07	2.390	1.060
20	516	444	1.33	321	1.44	2.223E + 08	3.824E + 11	−8.287E + 07	2.388	1.083
30	344	597	1.26	951	1.15	1.941E + 08	2.546E + 11	−8.115E + 07	2.376	0.913
60	172	533	1.33	502	1.36	1.039E + 08	1.269E + 11	−8.111E + 07	2.385	1.023
120	86	764	1.23	839	1.20	7.407E + 07	6.309E + 10	−8.100E + 07	2.372	0.976
240	43	775	1.27	797	1.26	3.843E + 07	2.027E + 06	−8.002E + 05	1.832	0.992
Hail contamination										
5	2064	300	1.40	30	2.09	3.450E + 08	0.028	1.695E + 03	1.001	1.493
10	1032	372	1.36	44	2.03	2.866E + 08	0.026	1.690E + 03	1.001	1.493
15	688	430	1.33	67	1.94	2.655E + 08	0.022	1.688E + 03	1.001	1.459
20	516	444	1.33	71	1.96	2.223E + 08	0.033	1.671E + 03	1.002	1.474
30	344	597	1.26	119	1.85	1.941E + 08	0.034	1.667E + 03	1.002	1.468
60	172	533	1.33	120	1.98	1.039E + 08	0.063	1.618E + 03	1.003	1.489
120	86	764	1.23	264	1.80	7.407E + 07	0.110	1.539E + 03	1.006	1.463
240	43	775	1.27	366	1.83	3.843E + 07	0.161	1.397E + 03	1.009	1.441

* Parameters found by regression of the true time series.
** Parameters found by regression of the erroneous time series.

Unauthenticated | Downloaded 04/15/21 10:46 AM UTC

ination errors the actual bias is larger than the calculated, while it is smaller for the synchronization error. These differences are possibly a result of the zero covariance assumption. Relative to Eq. (9), the negative covariance in the synchronization error reduces the bias, while the positive covariance increases the bias in the random and hail contamination errors. Also, it seems that the nonlinear regression model is more sensitive to hail contamination errors. The trend of the calculated bias is similar to the trend of the actual bias and fits the trend found using radar and gauge observations (Fig. 5c). Here again, the rapid decrease of the estimated b parameter is a result of the rapid reduction in the error variance with integration.

In summary, according to the above models, observational errors in reflectivity are responsible for the bias in the b parameter. The bias is often (but not always) positive (i.e., larger than 1). Large variance of reflectivities tends to reduce the bias, and large variance of errors tends to increase it. The covariance between reflectivity and reflectivity error also plays a role, but in a more complicated form. With increasing scale the variance of reflectivity errors drops relatively quickly (faster than the variance of reflectivity) and causes the reduction in bias (and in the estimated b) with scale. Both models assume independence of reflectivity errors in rain-intensity errors and therefore, the latter do not affect the bias according to the models. However, in reality such dependency possibly exists and the rain-intensity errors can affect the bias as well. In practice the regression of Z–R (linear or nonlinear) is done many times for the inverse relation; that is, R is the independent variable and Z is the dependent variable. In that case, the errors in rain intensities are the major cause of the bias.

c. The effect of model errors

Model errors result from incorrect assumptions about the functional relationship of Z and R. If the ''real'' Z–R relationship is not a power law, the optimal parameters are scale dependent, even if the data do not contain errors. This is demonstrated by generating simulated rainfall using a Z–R relationship based on the Window Probability Matching Method (WPMM). The WPMM method matches a specific Z to a specific R with the same percentile probability [see Rosenfeld et al. (1994) for more information]. We first derive the WPMM Z–R curve from rainfall intensities observed at a gauge located at the center of the watershed and from observed radar reflectivities at a pixel above the gauge. The upper threshold of 53 dBZ (hail threshold; see section 3c) is applied prior to generating the curve. The analyzed time series combines for the same radar pixel as the observed reflectivity (Z) with the simulated R from the WPMM Z–R curve. We examine scale dependency for 5–120 min using Z averaging. Figures 10a and 10b present the Z–R dataset and the fitted power-law curve at timescales of 5 and 30 min, respectively (please note that the log scale of the figures is for convenience, but the power-law parameters were derived using nonlinear regression). At the 5-min scale (Fig. 10a), the high slope of Z–R exists for the high Z values. That forces the fitted power law to have a relatively high exponent, which implies a low b value [Eqs. (1) and (2)]. When the curves are smoothed with integration (Fig. 10b), that effect is reduced and b increases.

It was found that the hail threshold affects the scale dependency of b. When the 53-dBZ threshold is used, the observed high intensities are all associated with this one value, which results in the high slope at the high end of the curve (Fig. 10a). As explained above, it implies a low-fitted b parameter that increases with scale (Fig. 10b). When no threshold is used, the observed high rain intensities are associated with gradually increasing reflectivities, which results in a low slope at the end part of the WPMM Z–R curve (Figs. 10c,d). Figure 11 shows the change in b with scale for several hail thresholds. In general, increasing the hail threshold results in higher optimal b parameters at the small scale, and this effect is reduced with integration. The effect of the hail threshold shown here emphasizes the importance of this parameter and indicates that the operational value of 53 dBZ might be too low in the current case. It should be emphasized, though, that changing the hail threshold value did not affect the trend of the scale dependency for observational errors (not shown).

5. Concluding remarks

In this paper we explored the scale dependency of the power-law Z–R parameters when estimated from radar reflectivity and rain gauge intensity data. In general, we found that model parameters are scale dependent if their optimal value, according to a given objective function, is changed with the time- and space scales at which the observed and calculated data are applied to this objective function. In our case, the data are observed (gauge based) and calculated (radar based) rainfall intensities, and the parameters are the multiplicative (a) and exponent (b) in the power-law Z–R relationship [Eq. (1)]. Scale dependency is investigated for 15 convective storms over the 149-km^2 semiarid, well-instrumented (74 gauges) USDA-ARS Walnut Gulch Experimental Watershed in the southwestern United States. The main findings of our study are summarized below.

1) Scale dependency was found for the power-law parameters. The experimental analysis shows that, in general b decreases and a increases with scale. The decrease of b with scale was found both for $R(Z)$ averaging and for Z averaging, but for the latter, b starts increasing for timescales larger than about 30 min.
2) Observational errors cause scale dependency of the power-law parameters. We show both experimentally

Unauthenticated | Downloaded 04/15/21 10:46 AM UTC

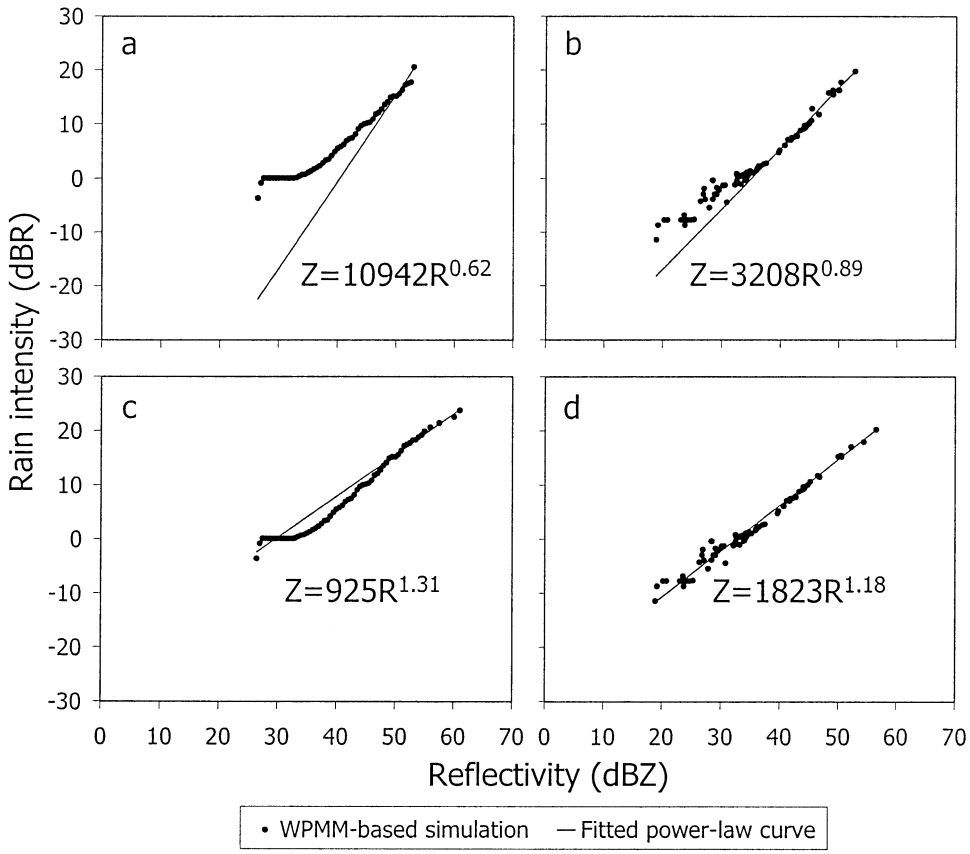

FIG. 10. WPMM-based *Z–R* and the best-fit power-law curve using the 53-dB*Z* hail threshold for (a) 5 min (original scale) and (b) 20 min; and without applying the hail threshold for (c) 5 min and (d) 20 min. The *Z* and *R* are presented in log scale using dB*Z* and dB*R* [=10 log(*R*)] units.

and using two rainfall models that the optimal *b* is often positively biased as a result of the observational errors. According to the models the bias is a function of the variance of the errors in reflectivity, the variance of reflectivities, and the covariance of the two. The decrease of *b* with scale, at least at the small scales, is due to rapid reduction in the variance of errors relative to the change in the variance of reflectivities.

3) Scale dependency can also be caused by model errors. It is shown that if we force the power-law *Z–R* relation on a nonpower-law dataset, the optimal parameters are changed with scale as the *Z–R* curve is smoothed. The trend in *b* is increasing or decreasing with scale.

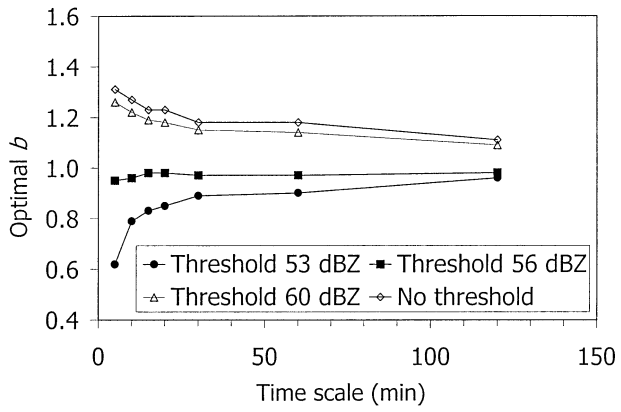

FIG. 11. Scale dependency of *b* that resulted from forcing a power-law relationship on a nonpower-law relation for different hail threshold parameters.

The scale dependency found here is based on analysis of radar and gauge observations, but in principle the same type of analysis could be conducted for distrometer-based data. Although much of the discrepancy is reduced when distrometer data are used, observational errors still exist and are expected to affect the determined *Z–R* relationship (Joss and Gori 1978; Campos and Zawadzki 2000).

The different sources of variance in observed radar–gauge *Z–R* datasets are well known and investigated in many papers (e.g., Zawadzki 1975; Austin 1987; Joss and Waldvogel 1990). However, the problem of scale dependency resulting from these sources of variance has not been fully examined. Despite the many difficulties,

Unauthenticated | Downloaded 04/15/21 10:46 AM UTC

radar–gauge data are often used in both research and operational settings for estimating rainfall intensities where the gauge information is only used to estimate the multiplicative parameter or both of the parameters of the power-law relationship. There are insufficient guidelines to suggest the appropriate scale at which radar and gauge rainfall should be compared, because different scales are used in research and operational algorithms. For example, the radar–gauge adjustment of the WSR-88D precipitation product is based on comparison of hourly gauge and radar rainfall amounts (Fulton et al. 1998), while the algorithm for ground validation rainfall for the Tropical Rainfall Measuring Mission (TRMM) satellite includes comparison of monthly rainfall amounts (Ciach et al. 1997; Marks et al. 2000). The current paper indicates that the selected timescales will likely affect the resulting parameters and, therefore, the radar rainfall estimates.

Based on the analysis presented, we cannot suggest strict time- and space scales to estimate parameters of radar-rainfall estimation algorithms. On one hand, our results indicate that parameters estimated using small-scale data are highly biased and that some space–time integration is needed to reduce the effect of observational errors. On the other hand, at very large scales, sample size and reflectivity variance might be too low and, again, the determined parameters are biased. We can, however, recommend caution when using parameters obtained from rainfall data at a given scale to estimate radar rainfall at a significantly different scale. This paper shows that scale dependency is a factor that should be taken into account in obtaining parameters' optimal value, in applying the parameters to estimate rainfall, and in validating the rainfall estimations [see Krajewski and Smith (2002) for more discussion on the validation issue]. The transferability of parameters between scales should be further studied, and additional investigations should be done, mainly directed to better understanding of the structure of errors in rain-intensity and reflectivity observations.

Acknowledgments. This research was funded by grants from the International Arid Lands Consortium (IALC; 00R-11) and the United States–Israel Binational Agricultural Research and Development Fund (BARD; FI-303-2000). The research is based upon work supported in part by the National Science Foundation Science and Technology Center for Sustainability of semi-Arid Hydrology and Riparian Areas (SAHRA; Agreement No. EAR-9876800) and by grants from the Hydrologic Laboratory of the National Weather Service (NA87WHO582 and NA07WH0144). We extend special thanks to Robert Maddox, Grzegorz Ciach, and David Bright for useful discussions and advice. This study would not have been possible without the dedication of the USDA-ARS Southwest Watershed Research Center, which provided financial support in development and maintenance of the long-term research facilities in Tucson and Tombstone, Arizona. Special thanks are extended to the staff located in Tombstone for their continued efforts. We thank Jeff Stone and David Bright for their help in reviewing the paper, Carl Unkrich for assistance in preparation of figures, and Anton Kruger for help with radar data visualization software.

REFERENCES

Atlas, D., D. Rosenfeld, and A. R. Jameson, 1997: Evolution of radar rainfall measurements: Steps and mis-steps. *Weather Radar Technology for Water Resources Management,* B. P. F. Braga and O. Massambani, Eds., UNESCO Press, 3–67.

Austin, P. M., 1987: Relation between measured radar reflectivity and surface rainfall. *Mon. Wea. Rev.*, **115,** 1053–1070.

Battan, L. J., 1973: *Radar Observations of the Atmosphere.* The University of Chicago Press, 324 pp.

Campos, E., and I. Zawadzki 2000: Instrumental uncertainties in *Z–R* relations. *J. Appl. Meteor.,* **39,** 1088–1102.

Ciach, G. J., and W. F. Krajewski, 1999: Radar–rain gauge comparisons under observational uncertainties. *J. Appl. Meteor.,* **38,** 1519–1525.

——, W. F. Krajewski, E. N. Anagnostou, J. R. McCollum, M. L. Baeck, J. A. Smith, and A. Kruger, 1997: Radar rainfall estimation for ground validation studies of the Tropical Rainfall Measuring Mission. *J. Appl. Meteor.*, **36,** 735–747.

——, M. L. Morrissey, and W. F. Krajewski 2000: Conditional bias in radar rainfall estimation. *J. Appl. Meteor.,* **39,** 1941–1946.

Creutin, J. D., and C. Obled, 1982: Objective analyses and mapping techniques for rainfall fields: An objective comparison. *Water Resour. Res.,* **18,** 413–431.

Draper, N. R., and H. Smith, 1981: *Applied Regression Analysis.* John Wiley and Sons, 709 pp.

Eagleson, P. S., N. M. Fennessey, W. Qinliang, and I. Rodriguez-Iturbe, 1987: Application of spatial Poisson models to air mass thunderstorm rainfall. *J. Geophys. Res.,* **92** (D8), 9661–9678.

Fulton, R. A., J. P. Breidenbach, D. J. Seo, and D. A. Miller, 1998: The WSR-88D rainfall algorithm. *Wea. Forecasting,* **13,** 377–395.

Goodrich, D. C., L. J. Lane, R. A. Shillito, S. N. Miller, K. H. Syed, and D. A. Woolhiser, 1997: Linearity of basin response as a function of scale in a semi-arid watershed. *Water Resour. Res.,* **33,** 2951–2965.

Habib, E., and W. F. Krajewski 2002: Uncertainty analysis of the TRMM ground-validation radar-rainfall products: Application to the TEFLUN-B field campaign. *J. Appl. Meteor.*, **41,** 558–572.

——, ——, and A. Kruger 2001: Sampling errors of fine resolution tipping-bucket rain gauge measurements. *J. Hydrol. Eng.,* **6,** 159–166.

Jameson, A. R., and A. B. Kostinski, 2001: Reconsideration of the physical and empirical origins of *Z–R* relations in radar meteorology. *Quart. J. Roy. Meteor. Soc.,* **127,** 517–538.

Jordan, P. W., A. W. Seed, and G. L. Austin, 2000: Sampling errors in radar estimates of rainfall. *J. Geophys. Res.,* **105** (D2), 2247–2257.

Joss, J., and E. G. Gori, 1978: Shapes of raindrop size distributions. *J. Appl. Meteor.*, **17,** 1054–1061.

——, and A. Waldvogel, 1990: Precipitation measurements and hydrology. *Radar in Meteorology,* D. Atlas, Ed., Amer. Meteor. Soc., 577–606.

Krajewski, W. F., and J. A. Smith, 2002: Radar hydrology: Rainfall estimation. *Adv. Water Resour.,* **25,** 1387–1394.

Kustas, W. P., and D. C. Goodrich, 1994: Preface to the special section on MONSOON '90. *Water Resour. Res.*, **30,** 1211–1225.

Maddox, R. A., J. Zhang, J. J. Gourley, and K. W. Howard, 2002: Weather radar coverage over the contiguous United States. *Wea. Forecasting,* **17,** 927–934.

Marks, D. A., and Coauthors, 2000: Climatological processing and

Unauthenticated | Downloaded 04/15/21 10:46 AM UTC

product development for the TRMM Ground Validation Program. *Phys. Chem. Earth,* **25B,** 871–875.
Marshall, J. S., and W. M. Palmer, 1948: The distribution of raindrops with size. *J. Meteor.,* **5,** 165–166.
Osborn, H. B., 1983: Precipitation characteristics affecting hydrologic response of southwestern rangelands. USDA-ARS Agricultural Reviews and Manuals ARM-W-34, 55 pp.
——, and W. N. Reynolds, 1963: Convective storm patterns in the southwestern United States. *Bull. IASH,* **8,** 71–83.
——, and R. B. Hickok, 1968: Variability of rainfall affecting runoff from a semiarid rangeland watershed. *Water Resour. Res.,* **4,** 199–203.
——, and L. J. Lane, 1972: Depth-area relationships for thunderstorm rainfall in Southeastern Arizona. *Trans. ASAE,* **15,** 670–673, 680.
——, and E. M. Laursen, 1973: Thunderstorm runoff in Southeastern Arizona. *J. Hydraul. Div. Amer. Soc. Civil Eng.,* **99,** 1129–1145.
——, and K. G. Renard, 1988: Rainfall intensities for Southeastern Arizona. *J. Irrig. Drain. Div., Amer. Soc. Civil Eng.,* **114,** 195–199.
——, L. J. Lane, and J. F. Hundley, 1972: Optimum gaging of thunderstorm rainfall in Southeastern Arizona. *Water Resour. Res.,* **8,** 259–265.
——, K. G. Renard, and J. R. Simanton, 1979: Dense networks to measure convective rainfall in the Southwestern United States. *Water Resour. Res.,* **15,** 1701–1711.
Renard, K. G., L. J. Lane, J. R. Simanton, W. E. Emmerich, J. J. Stone, M. A. Weltz, D. C. Goodrich, and D. S. Yakowitz, 1993: Agricultural impacts in an arid environment: Walnut Gulch case study. *Hydrol. Sci. Technol.,* **9** (1–4), 145–190.
Rosenfeld, D., D. B. Wolff, and D. Atlas, 1993: General probability-matched relations between radar reflectivity and rain rate. *J. Appl. Meteor.,* **32,** 50–72.
——, ——, and E. Amitai, 1994: The window probability matching method for rainfall measurements with radar. *J. Appl. Meteor.,* **33,** 682–693.
Sauvageot, H., 1992: *Radar Meteorology.* Artech House, 366 pp.
Seed, A. W., and G. L. Austin, 1990: Variability of summer Florida rainfall and its significance for the estimation of rainfall by gages, radar, and satellite. *J. Geophys. Res.,* **95** (D3), 2207–2215.
Sellers, W. D., and R. H. Hill, Eds., 1974: *Arizona Climate.* 2d ed. The University of Arizona Press, 616 pp.
Smith, J. A., and W. F. Krajewski, 1993: A modeling study of rainfall rate–reflectivity relationships. *Water Resour. Res.,* **29,** 2505–2514.
Smith, R. E., 1974: Point processes of seasonal thunderstorm rainfall: 3. Relation of point rainfall to storm areal properties. *Water Resour. Res.,* **10,** 424–426.
Steiner, M., J. A. Smith, S. J. Burges, C. V. Alonso, and R. W. Darden, 1999: Effect of bias adjustment and rain gauge data quality control on radar rainfall estimation. *Water Resour. Res.,* **35,** 2487–2503.
Trewartha, G. T., 1954: *An Introduction to Climate.* McGraw Hill, 402 pp.
Ulbrich, C. W., and L. G. Lee, 1999: Rainfall measurement error by WSR-88D radars due to variations in *Z–R* law parameters and the radar constant. *J. Atmos. Oceanic Technol.,* **16,** 1017–1024.
Zawadzki, I., 1975: On radar-raingage comparison. *J. Appl. Meteor.,* **14,** 1430–1436.
——, C. Desrochers, E. Torlaschi, and A. Bellon, 1986: A radar-raingage comparison. Preprints, *23d Conf. on Radar Meteorology,* Snowmass, CO, Amer. Meteor. Soc., 121–124.

Unauthenticated | Downloaded 04/15/21 10:46 AM UTC